Université Libre de Bruxelles
Faculté des Sciences Appliquées
CODE - Computers and Decision Engineering
IRIDIA - Institut de Recherches Interdisciplinaires
et de Développements en Intelligence Artificielle

Development of an Autonomous Swarm Construction System: Initial Steps

Touraj SOLEYMANI

Promoteur:

Prof. Marco DORIGO

Co-promoteur:

Dr. Vito TRIANNI

IRIDIA
Institut de Recherches
et de Développements Interdisciplinaires
en Intelligence Artificielle

Abstract

In this study, we develop a bio-inspired autonomous construction system in which self-contained ground robots build a protective barrier by means of deformable pockets (i.e., filled bags). We present a reactive and stochastic control algorithm based on bio-inspired mechanisms (stigmergy and templates) that takes advantage of deformable pockets for autonomous contruction. The control algorithm guides a single robot to build the structure by only employing odometry, vision, and proximity sensors. The control algorithm is also extended to be used in a swarm of robots. To demonstrate the feasiblity of the proposed system, real-robot and simulation experiments were carried out. We propose a statistical model to represent the structures built with deformable pockets. In addition, we provide a set of criteria for assessing the performance of the proposed system. Finally, we apply a scalability analysis to study the capabilities of the swarm construction system. The results show the viability of the proposed autonomous construction system in accomplishing the task.

To my parents

Contents

List of Figures

viii

List of Abbreviations and Symbols

Symbols

The followings are the basic notations and symbols used in this study:

x	lower-case letters with regular fonts represent scalars,
$\boldsymbol{x}$	bold lower-case letters represent vectors,
$\boldsymbol{X}$	bold upper-case letters represent matrices,
$\boldsymbol{r}_{ab}^{\vert c}$	the displacement vector of point a with respect to point b expressed in the coordinate system c,
$\boldsymbol{C}^{\vert ab}$	the transformation matrix between the coordinate system a and b.

Note that reference frames are distinguished from coordinate systems as the latter are only used for expressing the components of a vector. In this study, we adopt two reference frames: template reference frame t, and robot's body reference frame b; three coordinate systems: template coordinate system t, instantaneous coordinate system p, and robot's body coordinate system b (the letters of the coordinate systems always appear in the superscript after the line); two transformation matrices: transformation matrix between robot's body coordinate system and template coordinate system $\boldsymbol{C}^{\vert bt}$, and transformation matrix between instantaneous coordinate system and robot's body coordinate system $\boldsymbol{C}^{\vert pb}$; and four important points: template reference point t, robot's center of mass b, pocket's center of mass o, and deposition point d (the letters of the points always appear in the subscript).

Acknowledgements

First thank goes to my parents. Their love and belief in my abilities have helped me to progress through difficult moments.

I am so much grateful to my supervisor Marco Dorigo for his guidance and support. Being his student has been a great learning experience at different levels. I would like also to thank my co-supervisor Vito Trianni who provided me with valuable feedback that led to significant advances in my research. In addition, I would like to thank the committee members Mauro Birattari and Thomas Stützle.

Thanks to all of my former and current labmates: Gabrielle, Carlo, Manuele, Gianpiero, Tianjun, Alexandro, Nithin, Andreagioanni, Arne, Eliseo, Eric, Giovanni, Michele, Franco, Leslie, Lorenzo, Leonardo, Dhananjay, Gaetan, Roman, Jeremie, Manuel, Rehan, Anthony, and Tarik.

1

Introduction

Robots could be the only viable alternative for construction and manipulation tasks in environments that are hazardous or inaccessible for humans [Abderrahim and Balaguer, 2007], e.g. disaster areas, extraterrestrial surfaces, inside mines, and under seas. However, the employment of autonomous robots in these environments is still very challenging, and demands more research. Nature is one of the sources of inspiration that can help us in this regard. By observing nature, we can see how simple agents employ adaptive and robust solutions to construct in dynamic and unstructured environments. Examples of such constructions include beaver dams, termite mounds, caddisfly cases, bee hives, social weaver nests, spider webs, and anthill structures. Our goal is to develop an autonomous construction system, and we do so by taking inspiration from biology.

1.1 Autonomous construction

We define *autonomous construction* as a robotic task in which one or many autonomous robots repeatedly perform *grasping*, *transporting*, and *depositing* of material in order to build a structure.

To develop an autonomous construction system, we need to determine the following aspects of such a system:

i) The *task objective*, defined by the user, that specifies the form or function of the structure to be built.

ii) The *building material* of which the structure will be made up. Building materials can be categorized based on their physical properties into: rigid, deformable, and amorphous [Napp et al., 2012]. Examples of these categories include bricks, sandbags, and foam, respectively.

iii) The *autonomous robots* that build the structure, in terms of their sensing, processing, and actuation capabilities. There might be a single or multiple robots in the system, that can be ground, aerial, or undersea vehicles.

iv) The *control algorithm* that is implemented on the robot(s). There are two general approaches in artificial intelligence for designing the control algorithm: planning and reactive.

In our autonomous construction system, we employ ground robots with reactive control algorithms that build barriers by exploiting filled bags as deformable material. The motivations for this study and important aspects of the implemented system are provided in the following.

1.1.1 Task objective

The task objective in this study is to build a protective barrier against an unsafe environment. The real-world applications that motivate our task objective, and therefore this study, include building radiation shields after nuclear disasters such as the one that occurred recently in Japan, building lunar and Martian infrastructures like the one proposed in NASA's In-Situ Resource Utilization project [Smithers et al., 2007],

building emergency shelters after earthquakes [Khalili, 2011], and building levees against tsunamis. The functional and performance requirements that are imposed by these applications include radiation exposure reduction, structure integrity, impact resistance, low cost, fast and simple realization.

1.1.2 Building material

The building material must be chosen according to the task objective. In this work, we employ filled bags for building the protective barrier. The usage of this type of material is coherent with some recent researches. For example, Cal-Earth [Khalili, 2011] proposes the use of sandbags for emergency shelters, while NASA [Smithers et al., 2007; Cannon et al., 1990; Bell et al., 2011] proposes the use of regolith bags for building lunar habitats.

Filled bags are built by enclosing some amorphous material into fabric pockets, so that they maintain a certain degree of deformability. As a consequence, filled bags, henceforth deformable pockets, have the advantages of both rigid and amorphous materials, making them very appropriate for the autonomous construction of the aforementioned structures. In particular, they have the following features:

- Deformable pockets can conform to the shape of the environment in which they are placed. This allows to construct on rough and unleveled surfaces, and achieve packed structures. Furthermore, quick depositions of material is granted since the pockets, in contrast to rigid parts, do not require edge alignment. Quick deposition decreases the construction time and the sensing necessities of the robot.

- Deformable pockets can fill voids in a structure. This allows the structure to be built simultaneously from different points as the different pieces of the structure can seamlessly join one another. Conversely, building structures with

rigid parts requires deposition of the parts adjacent to the already situated ones. Deformable pockets can remarkably improve the efficiency in parallel deposition in multi-robot systems.

- By the use of deformable pockets, it is possible to exploit in situ materials of isolated areas or planets. Materials such as soil on earth and regolith on Moon, Mars, etc. are generally amorphous and cannot stay on their own. Deformable pockets are recognized as a simple, inexpensive, time-saving, and flexible approach for shaping these amorphous materials [Smithers et al., 2007; Khalili, 2011].

1.1.3 Autonomous robots

The robots must be equipped with the necessary sensors, processors, and actuators in order to be able to interact with the environment and manipulate the building material. In this study, robots are completely self-contained, i.e., sensing, processing, and actuation are onboard. Moreover, the employment of deformable pockets does not require high precision in positioning, and it allows us to use a simple manipulator.

1.1.4 Control algorithm

The control algorithm for autonomous construction must guide the robots to the right place (i.e., deposition point) for depositing the carried material. In our approach, inspired from biology, reactive behaviors exploit stigmergy and templates to achieve this goal:

- Stigmergy is the coordination of actions through modification and observation of the environment by the agents [Grassé, 1959]. In stigmergy, the current state of the environment is the result of the preceding building activities of the agents and stimulates the subsequent actions.

- Templates are heterogeneities of the environment (e.g., a temperature gradient) that can be recognized by the agents and that can influence their behavior [Theraulaz et al., 2003]. The final shape of the structure can be specified by the use of a template.

By exploiting the properties of the deformable pockets, we develop a simple stochastic control algorithm based on stigmergy and templates, that can compensate the uncertainties and unpredictabilities of the environment.

1.2   Autonomous swarm construction

The definition of autonomous construction can be extended to *autonomous swarm construction* by taking into account the characteristics of swarm robotics systems. As stated by Dorigo and Sahin: "*Swarm robotics can be loosely defined as the study of how collectively intelligent behavior can emerge from local interactions of a large number of relatively simple physically embodied agents*" [Dorigo and Sahin, 2004]. A swarm robotics system is characterized by the following properties:

- the number of robots is large,

- the robots are relatively simple,

- the robots cooperate with each other,

- the robots' controller is distributed,

- the interactions are local.

Swarm robotics systems can possess different functional properties. They can be *robust* against individual failures, *adaptive* against environment changes, *scalable* with respect to swarm size, and *parallel* in the work accomplishment. These properties make the swarm robotics systems very appealing for many applications,

5

in particular, autonomous construction. In this study, we ultimately move toward development of such systems. In fact, the aforementioned aspects of our autonomous construction system are designed in a manner that can be use in autonomous swarm construction.

1.3   Contributions

The contributions of this study are: 1) the investigation of the merits, feasibility, and performance of deformable pockets in autonomous construction through real-robot experiments; 2) the development of a bio-inspired, stochastic, and reactive control algorithm that exploits the properties of deformable material for autonomous construction in continuous environments; 3) the study of swarm autonomous construction by means of simulation experiments.

1.4   Outline

The remainder of this study is organized as follows: related work is discussed in Chapter 2. The scenario definition, specifications of the building material and of the robots, and the controller that is implemented on the robots are provided in Chapter 3. The metrics and real-robot experiments for a single robot are presented in Chapter 4. Simulation experiments and implementation of the algorithm for many robots are provided in Chapter 5. Finally, concluding remarks are made in Chapter 6.

2

Literature Survey

Autonomous construction has attracted the attention of several robotics researchers. In this brief survey, we limit ourselves to the description of those works that developed an autonomous construction system by employing real robots.

2.1   Reactive control algorithm

In a seminal work, Brooks et al. proposed a system made of twenty robots, equipped with a reactive behavior and a piling scoop for leveling soil on an artificial lunar surface [Brooks et al., 1990]. Melhuish et al. used six simple robots to sort pucks along a line considered as a template [Melhuish et al., 1999]. The structure was built by aligning pucks together, and was two dimensional. Wawerla et al. employed a single robot with reactive behaviors for building a two-dimensional structure made up of cardboard blocks [Wawerla et al., 2002]. In contrast to these works, our reactive control algorithm takes advantage of deformable pockets for building three-dimensional structures by stacking them.

2.2   Planning control algorithm

Petersen et al. developed a distributed planner for building three dimensional structures with a small mobile robot capable of moving on the building material, that is, custom-tailored blocks [Petersen et al., 2011]. Lindsey et al. employed up to three quadrotors and a central planner to build different framed structures out of beams and nodes [Lindsey et al., 2012]. Willmann et al. used four quadrotors to build a six meter tower with polystyrene modules [Willmann et al., 2012]. Finally, Wismer et al. adopted a single ground robot to build a roofed structure with polystyrene blocks [Wismer et al., 2012]. These works took advantage of a motion capture system for the precise estimation of states of robots and building parts, or of an external processing unit. Conversely, in this study we relax these necessities by exploiting the properties of deformable pockets.

2.3   Amorphous and deformable building material

Recently, Napp and Nagpal developed a distributed, reactive algorithm for deposition of foam as amorphous material in order to build a navigable ramp for robots [Napp and Nagpal, 2012]. Although an autonomous robot is not employed, they realized their system by using a remote controlled prototype robot and a scanning mechanism. Close to [Napp and Nagpal, 2012], Revzen et al. developed a modular robot capable of depositing foam in the environment [Revzen et al., 2011], and Khoshnevis proposed the "contour crafting" concept for building continuous structures by using a gantry system for deposition of amorphous material [Khoshnevis et al., 2010]. Napp et al. also studied the physical properties and functional requirements of a number of bio-inspired building materials for autonomous construction [Napp et al., 2012]. These studies demonstrate how the use of amorphous and deformable materials can open new ways to autonomous construction in unstructured environments. In this

paper, we study through real-robot experiments the feasibility and performance of a bio-inspired autonomous construction system with deformable pockets as building material.

3

Materials and Methods

In this chapter, we first introduce a scenario for the realization of our task objective in our laboratory arena. Then, we describe the deformable pockets and the robot used in our study. Finally, we provide the details of our control algorithm.

3.1   Task objective: build a protective barrier

The scenario is to build a barrier with a length of approximately one meter and width of approximately ten centimeters by stacking 30 pockets. This barrier provides a "safe" region in front of an "unsafe" region in the arena (see Fig. 3.1).

The arena is a rectangle of size 240 cm $\times$ 170 cm. Four green landmarks, situated in the arena for specifying the shape of the barrier, serve as template. Two green landmarks are also situated where the pockets are available to be grasped. Note that the global position of landmarks is not available to the robot.

The safe and unsafe regions are separated by an imaginary frontier called *boundary*. The boundary is made up of lines that connect the template landmarks to one another. We refer to these lines as *boundary lines*, and their length is denoted by d_{t_1}. Depending on the configuration of the landmarks, the boundary can have different
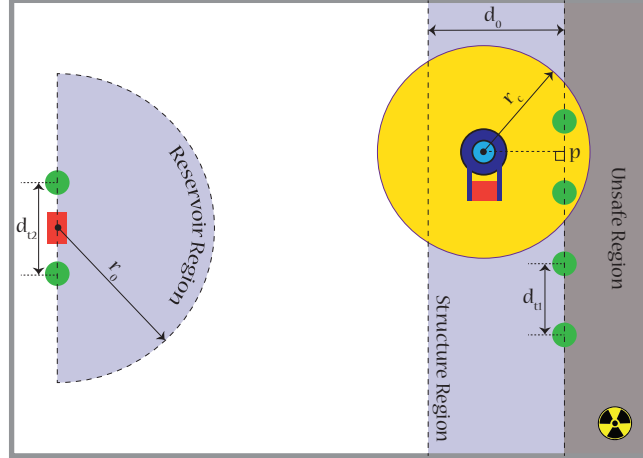
FIGURE 3.1: Scheme of the arena. The unsafe, the structure, and the reservoir regions are specified. The six small (green) circles represent the landmarks. The line that traverses the four landmarks on the right side is the boundary. The robot, represented as a dark (blue) circle in the structure region, is carrying a pocket (represented in red). The (yellow) circle around the robot shows the maximum range of the robot's omni-directional camera. Another pocket is placed in the reservoir region between the two landmarks.

shapes. In our case, it is linear.

We refer to the abstract region in which the deposition activity of the robot takes place as *structure region*. This region is defined in a way that guarantees that the robot can see at least two landmarks from any point of the structure region. The width d_0 of the structure region is therefore a function of the inter-landmark distance d_{t1} and the range r_c of the robot's omni-directional camera.

We call the abstract region in which the grasping activity of the robot takes place *reservoir region*. This region is defined by a semicircle of radius r_0. The radius value is set in such a way that the robot can see the two landmarks and the pocket from every point within the region. Therefore, r_0 is a function of the distance d_{t2} between the two landmarks and of the range r_c of the robot's omni-directional camera. The location of the pocket in the reservoir region is referred to as *reservoir location*. The new pockets are added manually at the reservoir location, placing their longitudinal

axis aligned with the two landmarks.

The robot should commute between the reservoir and the structure region, covering the approximate distance of 190 cm. It grasps pockets in the reservoir region, and deposits them in the structure region to build the structure following the template. In order to track the growth of the structure, we mount a Microsoft Kinect® on top of the structure region that captures the RGB and depth images of the structure at different time steps.

3.2 Building material: deformable pockets

The adopted pockets are passive, simple, and inexpensive. They were built by hand in short time and without high precision. A sample of these pockets is shown in Fig. 3.2. Each pocket is composed of a plastic bag filled with dry rice grains, in a manner that its shape can change to some extent under force exertion. A stripe of ferromagnetic metal is attached along the longitudinal axis of each pocket and serves for grasping by the robot, as described below. A red tape maintains this metal strip in position, and also makes the pocket visually recognizable by the robot's camera. Each pocket is 12 cm in length, 7 cm in width, and 1.5 cm in height; and weighs approximately 100 g. The size and weight of the pockets are chosen in a way that satisfies the requirements of the robot's manipulator.

3.3 Autonomous robot: the marXbot

We employ a marXbot [Bonani et al., 2010], a miniature modular mobile robot developed within the Swarmanoid project [Dorigo et al., 2013]. Fig. 3.2 illustrates this robot. The robot is 17 cm in diameter and 29 cm in height. The main sensors and actuators of the robot employed in this study are: an omni-directional camera, odometry encoders, differential treels (i.e., combinations of tracks and wheels), and a manipulator. The latter has 2 degrees-of-freedom: elevation and tilt [Magnenat

FIGURE 3.2: marXbot with its manipulator beside a pocket.

et al., 2012]. It can lay on the ground in order to detect a pocket, and can rise in order to pick up a pocket. At the base of the manipulator, there are 6 infrared proximity sensors, and a magnet that can be activated or deactivated. The robot is completely self-contained in sensing, processing, and actuation. There is no motion capture system feeding back the position of the robot and of the pockets, and no external computer executing the control algorithm.

Notice that the employment of metal and magnet in the design of the pockets and manipulator is solely a simple solution to the manipulation of pockets. This design could be substituted by any other design that allows the robot to reliably grasp and drop pockets.
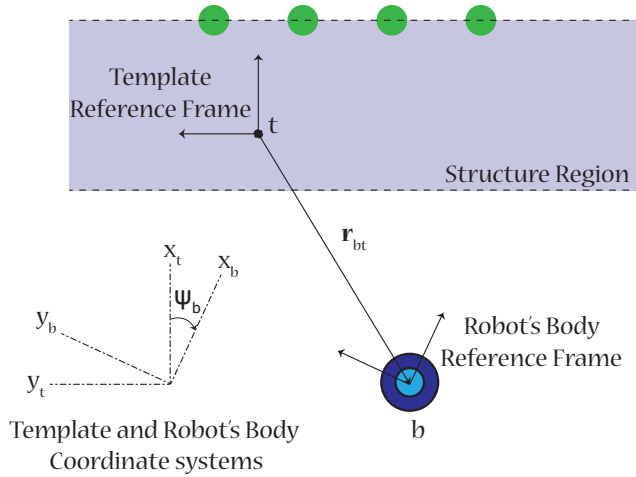
FIGURE 3.3: Template frame.

3.4 Control algorithm: bio-inspired behaviors

The control algorithm in this study is developed following a behavior-based approach. In our model, we define seven behaviors: explore, goto-reservoir, approach, pick-up, goto-structure, deploy, and drop. Among them, the deploy behavior is the most important one, and it is explained in detail.

Let us refer to a complete set of activities that the robot needs to perform from grasping to depositing a pocket as an iteration. In each iteration, the robot can employ different sensors for navigation. The relative position of the robot is computed by the odometry navigation equations, and the relative location of landmarks and pockets is obtained through the image processing of vision data. In addition, the proximity sensors are used to detect the nearby pockets and obstacles.

3.4.1 Odometry navigation

We introduce the *template frame*, a flexible reference frame with origin (i.e., reference point) any arbitrary point within the structure region, and with the positive direction
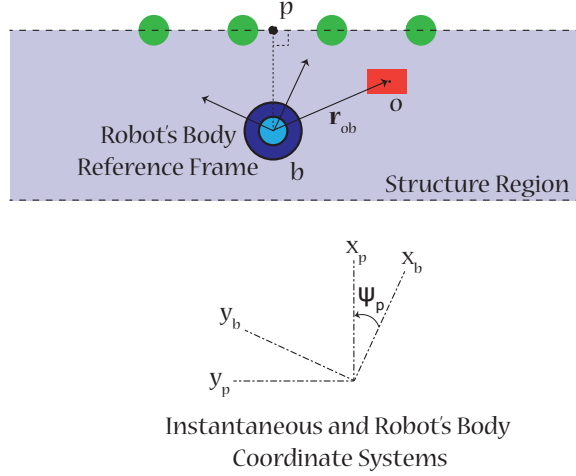
FIGURE 3.4: Instantaneous coordinate system.

of its x-axis perpendicular and pointing to a boundary line (see Fig. 3.3). The template frame is not fixed, but rather it is modified by the robot itself in each iteration after dropping a pocket. The robot exploits the template frame in its odometry navigation to move between the structure and the reservoir region.

The location of the robot with respect to the template reference point expressed in the template coordinate system is denoted by $\boldsymbol{r}_{bt}^{|t} = [x_{bt}^{|t} \quad y_{bt}^{|t}]^{\mathsf{T}}$, and its orientation is given by the angle ψ_b. Both are updated by solving the odometry navigation equations. The reservoir location is also expressed with respect to the template reference point and in the template coordinate system, and is denoted by $\boldsymbol{r}_{rt}^{|t}$. In order to execute the control commands in odometry navigation, the robot employs the transformation matrix between its body coordinate system and the template coordinate system $\boldsymbol{C}(\psi_b)^{|bt}$.

3.4.2   Visual navigation

When the robot is in the structure (or reservoir) region, the projection of the robot's location on the closest boundary line (or the line that connects the two landmarks

in the reservoir) is a point which is called *instantaneous projection point*. We refer to this point as the point p. Corresponding to the point p and with respect to the robot, we define the *instantaneous coordinate system* (see Fig. 3.4). The robot employs the instantaneous coordinate system in its visual navigation to navigate within the structure region (with an arbitrary boundary's shape) and the reservoir region. The transformation matrix between the robot's body coordinate system and the instantaneous coordinate system is denoted by $\boldsymbol{C}(\psi_p)^{|pb}$; where ψ_p is the angle of the point p with respect to the body coordinate system, and obtained from the image processing.

3.4.3 Behaviors

In the following we describe the behaviors of our reactive control algorithm:

Explore

The explore behavior allows the robot to acquire information about the structure and reservoir regions. The robot wanders in the arena at random, and avoids collisions with walls, landmarks, and pockets. When the robot enters the structure region, it constructs the template frame, and initializes it. When it enters the reservoir region, it saves the reservoir location with respect to the template reference point. However, if the reservoir region is detected sooner than the structure region, the robot updates the reservoir location in the template frame after it enters the structure region. Once both structure and reservoir regions are detected, the goto-reservoir behavior is activated.

Goto-reservoir

In the goto-reservoir behavior, the robot uses odometry navigation to reach the reservoir region. When the robot enters this region, the behavior proceeds to the approach behavior.

Approach

In the approach behavior, the robot uses visual navigation to detect the two land-marks and the pocket. For the alignment of the manipulator with the pocket, the approach trajectory should roughly be normal to its longitudinal axis. Therefore, the robot first moves toward a specified point in front of the pocket, then it lowers the manipulator and moves toward it. When the distance between the robot and the pocket becomes small enough, the pick-up behavior is activated.

Pick-up

In the pick-up behavior, the robot moves forward until it detects the pocket through the proximity sensors of the manipulator. Then, it raises the manipulator to the top of the pocket, activates the magnet, and picks up the pocket. At this time, the robot saves the current location as the reservoir location, and the goto-structure behavior is activated.

Goto-structure

In the goto-structure behavior, the robot uses odometry navigation in order to reach the structure region. When the robot enters this region, the deploy behavior is activated.

Deploy

The deploy behavior is the main part of the control algorithm. It must decide on the deposition point and guide the robot toward it. In a three dimensional space, the deposition point can be specified with respect to the template frame by its six coordinates: $x_{dt}^{|t}$, $y_{dt}^{|t}$, $z_{dt}^{|t}$, ψ_{dt}, θ_{dt}, and ϕ_{dt}. One can show that in construction with pockets, and in presence of gravity, the decision space regarding deposition points becomes two-dimensional; the height is specified directly by the structure itself, and

the orientation of pockets is not required thanks to the pockets' deformability. It means that the deploy behavior has to solely decide on $x_{dt}^{|t}$ and $y_{dt}^{|t}$. Eventually, we expect a three-dimensional structure to emerge when pockets are accumulated in a two-dimensional domain.

Assuming that the robot is in the structure region, the vision sensor can detect a part of the template and of the structure. First, the robot randomly chooses between the right and left directions. Then, it moves along the boundary at a specified distance from it. If the robot reaches one of the ends of the boundary, it turns around and continues moving in the opposite direction.

Let $\mathcal{N}$ denote the set of all pockets in the arena at time t, and $\boldsymbol{r}_{o_i b}^{|b}$ the location of pocket i with respect to the robot expressed in the robot's body coordinate system (see Fig. 3.4). The set of visible pockets is defined as

$$\mathcal{N}_v = \{j \in \mathcal{N} : |\boldsymbol{r}_{o_j b}^{|b}| \leqslant r_c; \ o_j \text{ is not occluded}\} \tag{3.1}$$

where $\boldsymbol{r}_{o_i b}^{|b}$ for all $i \in \mathcal{N}_v$ is given by the image processing on the vision data.

One can express the location of each visible pocket with respect to the robot in the instantaneous coordinate system by the transformation $\boldsymbol{r}_{o_i b}^{|p} = \boldsymbol{C}^{|pb} \boldsymbol{r}_{o_i b}^{|b}$ with the components $\boldsymbol{r}_{o_i b}^{|p} = [x_{o_i b}^{|p} \quad y_{o_i b}^{|p}]^{\intercal}$ for all $i \in \mathcal{N}_v$. At each time step, while moving along the structure, the robot calculates these components for every visible pocket. By using the y-component of the visible pockets' location, we can define the set of influential pockets as

$$\mathcal{N}_f(\delta) = \{j \in \mathcal{N}_v : |y_{o_j b}^{|p}| \leqslant \delta\} \tag{3.2}$$

where δ is an adjustable parameter called influential range. The probability of choosing the current y-component of the location of the robot in the template reference frame $y_{bt}^{|t}$ for the deposition (i.e., $y_{dt}^{|t}$) is defined as

$$P\left(y_{dt}^{|t} = y_{bt}^{|t}; \ n_f(\delta_1)\right) = \frac{k_1}{1 + \alpha^2 n_f(\delta_1)^2} \tag{3.3}$$

18

where k_1 is a scaling factor, α is an arbitrary constant, and $n_f(\delta_1) = |\mathcal{N}_f(\delta_1)|$ is the size of the set of influential pockets for the influential range δ_1. Equation (3.3) means that if the number of influential pockets in an area is low, the probability of depositing the carrying pocket there is high and *vice versa*. This mechanism is analogous to a negative feedback and serves to fill voids along the length of the structure. Besides, the deposition at $y_{bt}^{|t}$ is inhibited if the height of the structure increases more than a specified value.

Once the robot decided on $y_{dt}^{|t}$, it turns and moves toward the boundary line. At each time step, while it is moving in the direction of the point p, the robot calculates the x-component of the mean location of the influential pockets with respect to the manipulator as

$$\mu_x(\delta_2) = \frac{1}{n_f(\delta_2)} \sum_{j \in \mathcal{N}_f(\delta_2)} x_{o_j b}^{|p} - d_m \tag{3.4}$$

where d_m is the distance between the center of the manipulator and of the robot, and $n_f(\delta_2) = |\mathcal{N}_f(\delta_2)|$ is the size of the set of influential pockets for δ_2. The probability that the robot selects the current x-component of its location in the template frame $x_{bt}^{|t}$ for the deposition (i.e., $x_{dt}^{|t}$) is defined as

$$P\big(x_{dt}^{|t} = x_{bt}^{|t};\ \mu_x(\delta_2)\big) = k_2 \exp\Big(-\frac{\mu_x(\delta_2)^2}{\sigma^2}\Big) \tag{3.5}$$

where k_2 is a scaling factor and σ is a constant. Equation (3.5) means that the robot deposits the carrying pocket where the density of pockets along the width of the structure is higher. This mechanism is similar to a positive feedback and maximizes the compactness of the structure along its width. In addition, the deposition at $x_{bt}^{|t}$ is forced if the robot gets close to the boundary line more than a specified value. Once the robot decided on $x_{dt}^{|t}$, it stops, and the drop behavior is activated.

19

Drop

In the drop behavior, the robot deactivates the magnet of the manipulator and lets the pocket drop thanks to the gravitational force. The robot then reinitializes the template frame based on its current state, and updates the reservoir location in the new template frame. This eliminates the accumulated noise in the odometry data from the previous iteration. This completes one iteration in the construction, and control goes to the goto-reservoir behavior in order to start a new iteration.

3.4.4   Inter-robot interactions

The proposed control algorithm is developed in a manner that can be easily implemented on a swarm of robots. However, to do so some consideration and modification of the control algorithm regarding inter-robot interactions are necessary.

Distributed reference frame

We recall that the template frame is a reference frame that is defined independently for each robot. This frame plays an important role in decentralization of the control algorithm since the robots do not require to be equipped with a common reference frame for their navigation. The template frame is initialized by each robot through a search and exploration process in the explore behavior, and it is then updated at the end of each iteration. Although the template frame is constructed, initialized, and updated independently by each robot, it organizes the construction activities of the robots in the autonomous swarm construction.

Interference resolution

Another important issue in autonomous swarm construction is conflict resolution between robots. The robots in the swarm encounter each other many times during their activities. In these encounters, the trajectories of the robots may intersect with

one another. Thus, a *resolution mechanism* is required to avoid the collisions of robots, and to allow them to move toward their own goals. The way the resolution mechanism works depends on the behavior of the robot.

If the robot is in the explore, goto-reservoir, or goto-structure behavior, the resolution mechanism simply changes the velocity direction of the robot away from the collision point. If the robot is in the approach behavior, it forces the robot to wait for a while if another robot (that is closer to the pocket) is detected approaching the pocket.

The resolution mechanism in the deploy behavior is more complex. In autonomous construction with mobile robots, in order for the robots to find an appropriate place for the deposition, it is necessary to move around and visit the structure (or boundary of the structure). Therefore, a path in the vicinity of the structure is required to be defined, and be used by the robots. The robots enter this path, move along it until they find the appropriate place, deposit the building material, and then exit the path. Note that in our approach deposition is a stochastic process, and the robots do not necessarily choose the first appropriate place they visit. This allows the robots to explore and build the structure somehow uniformly, and also reduces the concentration of the robots in one area.

The boundary in general can be closed (e.g., a rectangle) or open (e.g., a line). If the boundary is closed, one can consider a single path with one traffic direction around the boundary that the robots can use to visit the structure. In this case, the entrance to and exit from the path can be chosen in any point. Now, suppose that the boundary is open and the structure is to be built only on one side of the boundary. We will investigate the alternative solutions for this condition as this is the case considered in our scenario.

One solution consists in using a single path with one traffic direction. It this case, the entrance must be at one of the ends of the path (starting point), while the exit

can occur in any point of the path. This solution is not effective when the boundary is very long because the robots have to always begin from the starting point and visit the built part of the structure.

Another solution is to consider a single path in which both the traffic directions are allowed, and the entrance and exit are admissible in any point of the path. In this solution, the robots may bypass or make a u-turn when they meet each other. We observed in preliminary experiments that this approach soon reaches a saturation when the size of the group increases, so it is not effective.

In our work, we propose a double path solution in which each of the paths takes one traffic direction. In this case, one path is closer to the boundary with respect to the other one. We call the closer one the main path with right to left traffic direction, and the further one the auxiliary path with left to right traffic direction. In order to reduce the traffic, we assume that the entrance is always into the auxiliary path, and deposition is only allowed when the robot is in the main path. Once the robot enters the auxiliary path, it checks whether there is any robot on its left side. If there is no robot, it turns and enters the main path. Otherwise, it continues until the left side becomes free. When on the main path, the robot uses the deploy behavior to find an appropriate place for deposition, and once found, it drops the pocket. Next, the robot resumes motion on the main path until its left side becomes free, in order to switch to the goto-reservoir behavior and to move toward the reservoir. Note that if a robot stops in the main path, for example for dropping a pocket, the other robots behind it also stop temporarily. This resolution mechanism is expected to reduce the interference between robots within the structure region.

Stochastic direction change

Based on the resolution mechanism, the robots can deposit pockets when they are in the main path, and within the main path they can only move leftward. Unfortunately,

this makes the probability of visiting the right side of the structure less than the left side, and eventually creates an asymmetry in the structure. To remove this behavior, we devise a mechanism named *loop mechanism*. In the loop mechanism, the robot probabilistically decides to enter the auxiliary path from the main path and *vice versa*. Let λ denote the direction decision, that is, the robot's decision for being in a particular path. The direction decision can be $\lambda = 1$, that corresponds to the robot's decision for being in the main path, or can be $\lambda = -1$, that represents the robot's decision for being in the auxiliary path. The probability of changing the path at each time is defined as

$$P(\lambda \to -\lambda) = \tau_\lambda \tag{3.6}$$

where $\tau_\lambda \in [0, 1]$ is a parameter. The mean traveled distance along a path is adjustable by changing τ_λ. The loop mechanism results in a uniform probability of visiting any part of the structure in the main path. Note that when a robot reaches the end of the boundary, it is forced to enter to the auxiliary path, but it can later come back to the main path thanks to the loop mechanism.

<div align="right">

4

</div>

Metrics and Real-Robot Experiments

In this chapter, we evaluate the performance of the proposed autonomous construction system. We first introduce a statistical model to investigate the properties of the structures built out of pockets. Then, we provide the results of our real-robot experiments, according to a set of criteria for assessing the quality of the built structures.

4.1   Statistical model of the structure

In order to study the quality of the decisions made regarding deposition points $(x_{dt}^{|t}$ and $y_{dt}^{|t})$, we should analyze the effect of these decisions on the resulting structure after a finite number of depositions.

One way for describing the structure is to use height functions as suggested for amorphous materials in [Napp and Nagpal, 2012]. The height function $h(\boldsymbol{x}) : \mathbb{R}^d \rightarrow \mathbb{R}_{\geqslant 0}$ can be defined by the height of the exterior surface of the structure over the d-dimensional construction domain.

With pockets, a more appropriate way for representing the emerged structure

<div align="center">

24

</div>

and analyzing the quality of the decisions is to study their distribution in space. This is because pockets are discrete and countable objects, and additionally there is some inherent uncertainty in the deposition that can be grasped only by means of a statistical model. Accordingly, we propose *kernel density estimator* as a method to obtain a statistical model for structures with pockets. Kernel density estimation is a non-parametric approach for estimating the density function of a finite set of data samples [Wand and Jones, 1995]. Let $\boldsymbol{x}_i \in \mathbb{R}^d$ denote the d-dimensional location of pocket i in an arbitrary coordinate system for all $i \in \mathcal{N}$. The multivariate kernel density function $\hat{f}_{\boldsymbol{H}}(\boldsymbol{x}) : \mathbb{R}^d \to \mathbb{R}_{\geqslant 0}$ of a structure with pockets after n depositions is defined as

$$\hat{f}_{\boldsymbol{H}}(\boldsymbol{x}) = \frac{1}{n} \sum_{i=1}^{n} K_{\boldsymbol{H}}\big(\boldsymbol{x} - \boldsymbol{x}_i\big) \tag{4.1}$$

where $K_{\boldsymbol{H}}(\boldsymbol{x})$ is

$$K_{\boldsymbol{H}}(\boldsymbol{x}) = |\boldsymbol{H}|^{-1/2} \ K(\boldsymbol{H}^{-1/2}\boldsymbol{x}) \tag{4.2}$$

where $\boldsymbol{H}$ is a symmetric positive-definite $d \times d$ matrix called the bandwidth matrix and $K(\boldsymbol{x})$ is the kernel function. The kernel function is a symmetric function that satisfies

$$\int_{\mathbb{R}^d} K(\boldsymbol{x})d\boldsymbol{x} = 1 \tag{4.3}$$

We suppose that the kernel in our study is a normal density function as

$$K(\boldsymbol{x}) = \frac{1}{(2\pi)^{d/2}} \exp\big(-\frac{1}{2}\boldsymbol{x}^\mathsf{T}\boldsymbol{x}\big) \tag{4.4}$$

In order to calculate the kernel density function for the whole structure, we only require the two dimensional location of the center of mass of pockets. We associate a kernel to each of these centers of mass. Therefore, each deposition is considered as one kernel, and the accumulation of pockets is modeled by the summation of the corresponding kernels. Since the decisions on deposition points are probabilistic,

a density function accounts for the probability distribution of these decisions. A density function also takes into account the uncertainties in the shape and final location of the pockets.

4.2   Performance criteria

To provide a quantitative evaluation of the proposed approach, we define four criteria to investigate the quality of the structure and of the deployment algorithm. Assume that we have the two dimensional locations of the pockets $[x_i, y_i]^\intercal$ for all $i \in \mathcal{N}$ after n depositions. We define these criteria in the following.

4.2.1   Uniformity deviation

The uniformity deviation measures the difference between the pockets' distribution along the length of the structure and a uniform distribution. To measure the uniformity deviation after n depositions, we calculate the normalized integral of the absolute difference between the univariate kernel density and the uniform density along the length of the structure as

$$u_d(n) = \frac{1}{2A} \int_a^b \big| f_h(x) - f_u(x) \big| dx \tag{4.5}$$

where a and b are the extremities of the structure, $f_u(x)$ is the uniform distribution, and A is the integral of the kernel density function over the interval $[a, b]$ (the scalar 2 in the denominator is used only normalization). By construction, the following property holds in the interval $[a, b]$:

$$\int_a^b f_u(x) = \int_a^b f_h(x) = A \tag{4.6}$$

resulting in a theoretical maximum uniformity deviation of 1. As a consequence, low values of $u_d(n)$ correspond to more uniform structures.

4.2.2 Integrity deviation

The integrity deviation represents the cohesion of the structure along the width. It is defined as the standard deviation of the pockets' distribution along the width of the structure after n depositions

$$i_d(n) = \sqrt{\frac{1}{n-1} \sum_{i=1}^{n} (y_i - \bar{y})^2} \tag{4.7}$$

where $\bar{y}$ is the mean of the y-component of the pockets' locations. Low values of $i_d(n)$ indicate high coherence of the structure along the width.

4.2.3 Maximum gap

The maximum gap can represent the narrowest part of the structure. It is defined as the maximum distance between two adjacent pockets along the length of the structure after n depositions

$$d_m(n) = \max \left\{ d_{ij} : i, j \in \mathcal{N}; \ x_j \geqslant x_i; \ \forall k \in \mathcal{N} : x_k \geqslant x_i \rightarrow x_k \geqslant x_j \right\} \tag{4.8}$$

where d_{ij} is the distance between the x-components of the location of the pockets i and j. Low values of $d_m(n)$ are desirable.

4.2.4 Construction time

The last criterion is construction time, that is, the time required for depositing n pockets, denoted by $t_c(n)$.

4.3 Real single robot experiments

We employed one robot for the real-robot experiments. Twenty trials were carried out, and in each trial the robot successfully built the structure without any failure.

We provide the detailed results of one selected trial. Fig. 4.1 illustrates the construction process through some snapshots of the structure at different time steps.
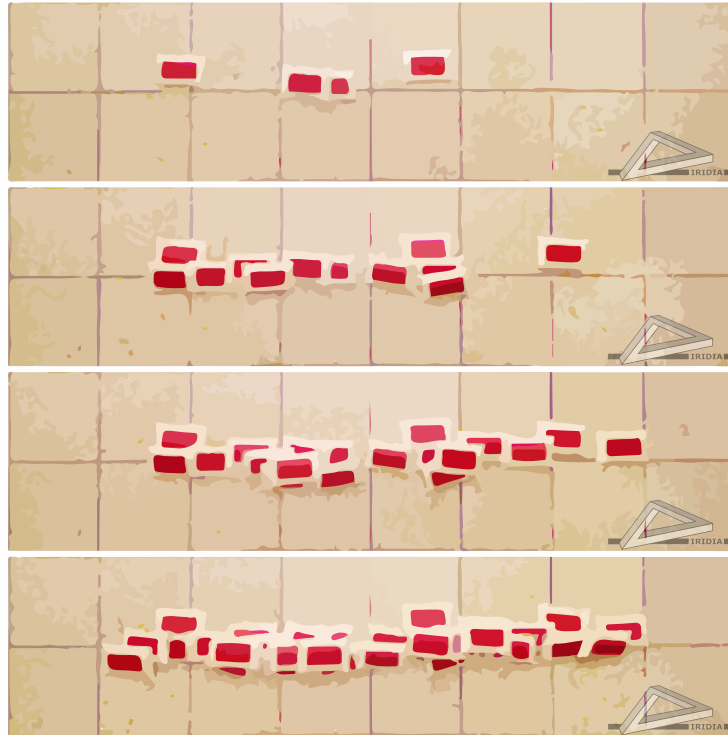
FIGURE 4.1: Snapshots of the structure at different time steps. From top to down: a) $t = 261$ s, $n = 4$, b) $t = 869$ s, $n = 12$, c) $t = 1425$ s, $n = 19$, d) $t = 2366$ s, $n = 30$.
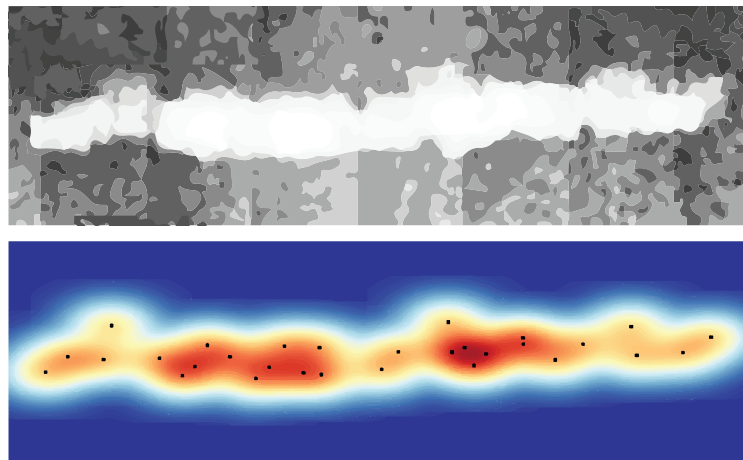
FIGURE 4.2: Top: Depth map of the final structure for the selected trial. Bottom: Bivariate kernel density function of the final structure for the selected trial.
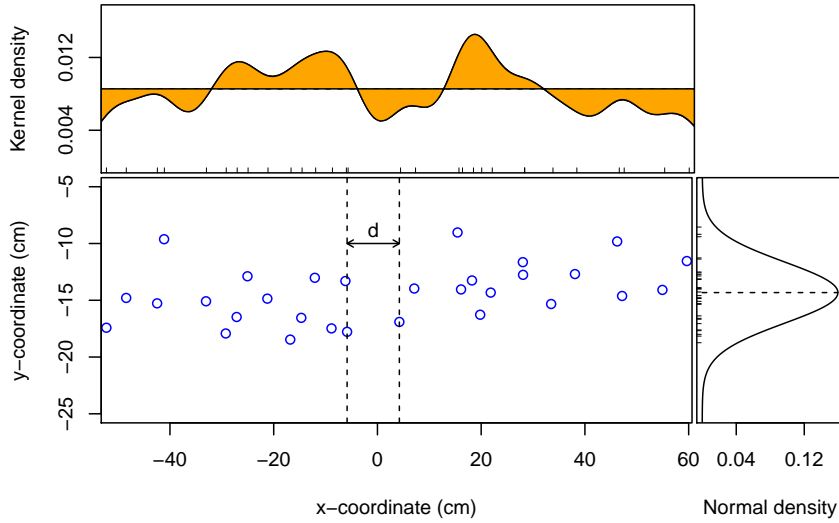
FIGURE 4.3: Bottom left: two dimensional distribution of pockets of the final structure for the selected trial. The maximum gap d is shown in the plot. Top: Univariate kernel density function along the length of the structure compared to the corresponding uniform density function. The uniform deviation is the integral of the colored area. Bottom right: normal density function fitted to the distribution of pockets along the width of the structure. The integrity deviation is the estimated standard deviation of this function.

After each deposition, the depth image of the structure was captured by using a Microsoft Kinect®. The depth map representing the height function is illustrated in Fig. 4.2 for the final structure. Through image processing, by comparing each two consecutive depth images of the growing structure, the last deposited pocket was recognized, and its two dimensional location in an absolute coordinate system was extracted. Therefore, the two dimensional locations of the pockets $[x_i, y_i]^\intercal$ for all $i \in \mathcal{N}$ after n depositions are available for our analysis. We computed the bivariate kernel density function for the final structure by choosing a diagonal bandwidth matrix with elements h_1 and h_2 respectively for the x- and y-directions. Fig. 4.2 depicts the heat map diagram of the bivariate kernel density function. We note a close correspondence between the height function and the kernel density function, which supports the choice of the latter as a model of the structure.
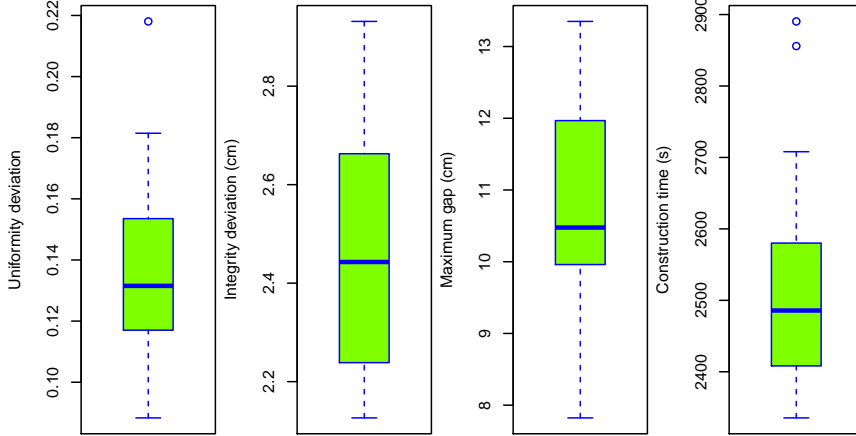
FIGURE 4.4: From left to right respectively: box plot diagram of the uniformity deviation, integrity deviation, maximum gap, and construction time for 20 real-robot experiments.

The performance criteria were evaluated for all trials. In the specific case of a sample trial (see Fig. 4.3), their values for the final structure are: $u_d(30) = 0.13$, $i_d(30) = 2.50$ cm, $d_m(30) = 10.07$ cm, and $t_c(30) = 2366$ s.

Fig. 4.4 reports the performance of the autonomous construction system based on the four criteria for 20 trials. Here, we discuss the median of the criteria as their dispersion is acceptably small.

The median of uniformity deviation is $\tilde{u}_d(30) = 0.13$, which shows 13% deviation from the uniform distribution. This indicates that the robot built the structures uniformly obtaining a roughly constant height.

The median of integrity deviation is $\tilde{i}_d(30) = 2.44$ cm which suggests that pockets are normally placed in the range ± 7.32 cm, that is $\pm 3 \times \tilde{i}_d(30)$. This roughly corresponds to twice the width of a pocket, meaning that the built structure are very coherent, integrated, and packed.

The median of maximum gap is $\tilde{d}_m(30) = 10.48$ cm, which corresponds to a max-

imum edge to edge distance between adjacent pockets along the length of -1.52 cm (obtained from $\tilde{d}_m(30) - 12$ where 12 cm is the length of each pocket). The minus sign represents the pocket overlapping. It indicates that the robot filled most of the voids in the structure. Although in the worst case still a small void exists, by increasing the number of depositions it can be covered.

Finally, the median of construction time is $\tilde{t}_c(30) = 2486$ s. This means that each iteration takes about 83 s in average; that is $\tilde{t}_c(30)/30$. Considering the average speed of the robot (≈ 10 cm/s), the distance between the reservoir and structure region, and the average time for grasping one pocket (≈ 15 s), the robot spends approximately 30 s for each deposition in average.

Overall, by analyzing the structures built in all trials according to the above metrics, we can conclude that our autonomous construction system is appropriate for the pockets. The reactive, bio-inspired behavior we developed provides a very simple deposition mechanism, which can exploit the properties of deformable pockets to provide uniform, integrated, void-free structures.

5

Simulation Experiments and Scalability

In this chapter, we study autonomous swarm construction through simulation experiments. The reason for resorting to simulation is that it allows us to study the performance of the multi-robot system before a number of real robots becomes available. In fact, the real robots with their manipulators are currently being manufactured; the one used in this study is the only prototype. The simulator employed in this work is called ARGoS, a high fidelity multi-robot simulator developed within the Swarmanoid project [Pinciroli et al., 2012]. In the following, we first present single robot experiments tailored to validate the simulation model, followed by multi-robot experiments to demonstrate autonomous swarm construction. Finally, we study the effects of increasing the swarm size on the performance of the system.

5.1   Validation of the simulation

The robot MarXbot has been simulated, tested, and verified in the simulator with all of its important subsystems in a number of previous studies [Ducatelle et al., 2011; Pini et al., 2013]. However, for the purpose of this study, a simulation of the pockets has to be developed. Precise simulation of deformable pockets needs

extensive modeling and computations. In this section, our goal is to find a simple and appropriate model for deformable pockets that can match functional properties of the real pockets.

The interaction of the robots with the pockets is mainly based on visual perception. In our simulator, the omni-directional camera is modeled geometrically. Thus, the distance and angle of the center of mass of each object (acquired through image processing in reality), are available by geometric calculations. To make the camera model more realistic, we add noise to the output data of the camera. However, we need to simulate the occlusion of the stacked pockets. To this end, we employ a simple model that associates a value, percentage of occlusion, to each pocket. When other pockets are stacked on top of a pocket, this value decreases as a function of the occluded area. Eventually, under a specific threshold, we consider that the pocket is not visible anymore by the robot.

Different occlusion thresholds can change the quality of the final structure in the simulation. In the simplest condition, if we do not take into account the occlusion, all pockets in the structure will be visible by the robots. This has an influence on the deploy behavior of the robots. We need therefore to examine the effect of the occlusion threshold on the results of the simulation.

We ran simulations with a single robot with the same setup used in the real-robot experiments introduced earlier. We evaluated the four criteria based on the locations of the pockets in the final structure. Fig. 5.1 reports the performance of the construction algorithm for a single robot in simulation with different occlusion threshold values and the results of real-robot experiments. These data are based on 200 trials for the simulation experiments and 20 trials for real-robot experiments. By comparison, among different models, we choose the simulation model with the occlusion threshold 75% which shows a better closeness in all criteria to the real-robot experiments. The simulation results for a single robot matches very well with
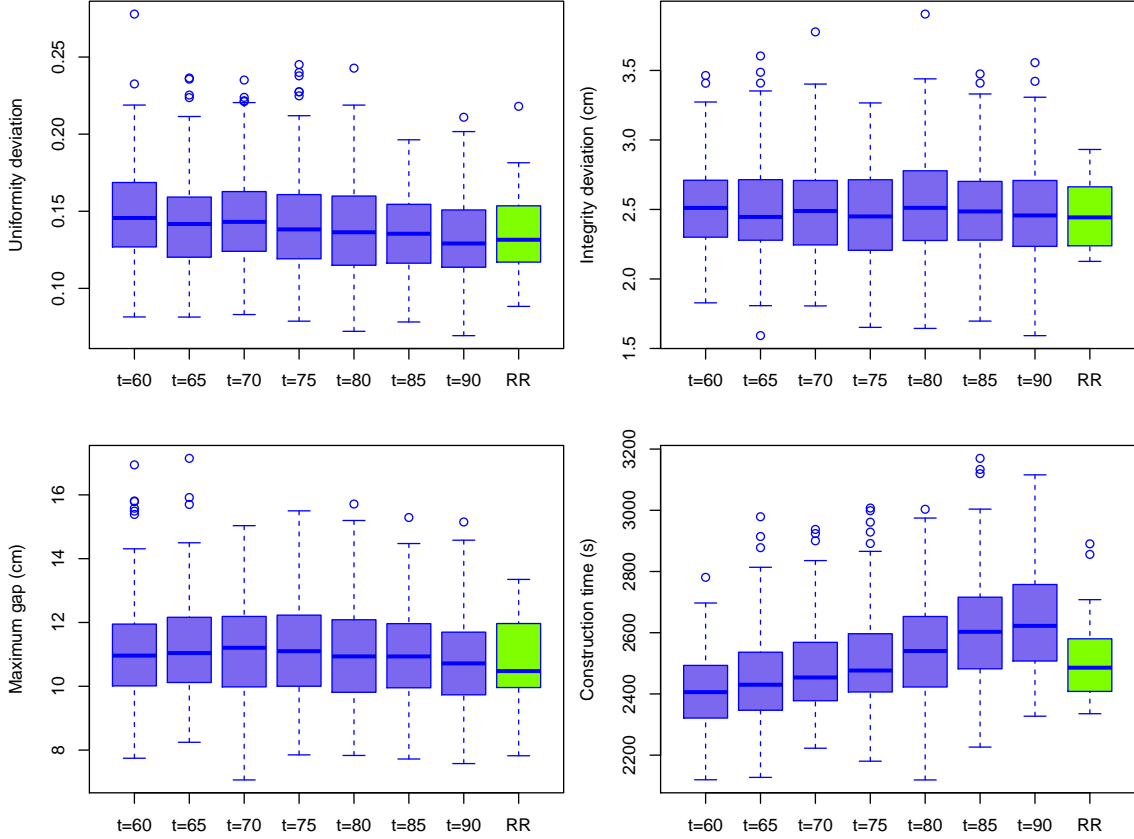
FIGURE 5.1: The results of the four criteria in the simulation experiments with different occlusion threshold values compared with those of the real-robot experiments (both with a single robot).

the results of real-robot experiments for the same scenario. Therefore, we accept our simulated model, and we use it also for multi-robot simulation.

5.2 Scalability analysis

Once that an appropriate simulation model has been devised, we study autonomous construction with many robots. The main difference between multi-robot and single robot experiments is the presence of interference between robots. Interference can decrease the performance of each robot. However, we expect that by employing many robots the overall performance of the system will increase. To study this effect, we
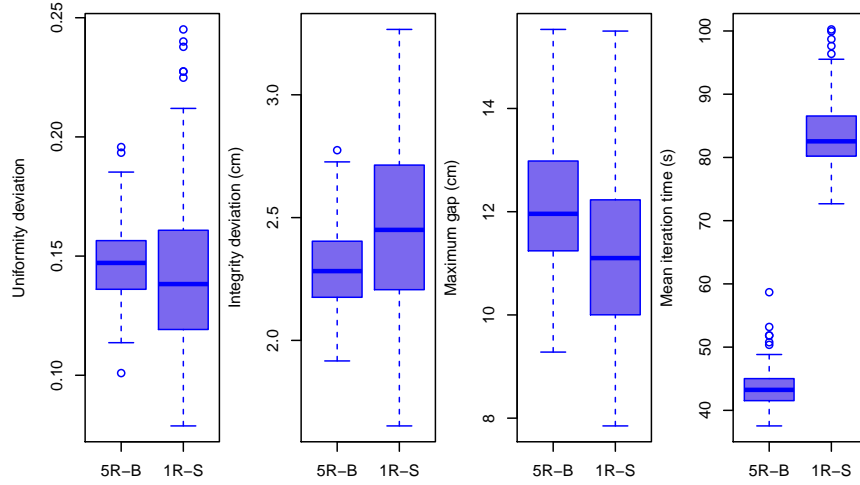
FIGURE 5.2: The results of the four criteria in the simulation experiments with 5 robots in the big arena compared with those of the simulation experiments with 1 robot in the small arena (both with the same occlusion value 75%).

need to analyze the performance of autonomous construction with different group sizes. That is, we perform a scalability analysis.

We first change the setup of the experiments in terms of size and configuration of the arena so as to accommodate more robots. The size of the arena is changed to 400 cm × 600 cm. As before, the unsafe region is in one side of the arena and the reservoir is placed in the other side. The boundary is now made of 20 landmarks that form a 350 cm straight line. We also increase the number of reservoirs to 5. Each of them is still specified by two landmarks at the sides of each pocket, as in the single robot experiments. The distance between the reservoir and structure regions is of approximately 330 cm. In this setup 112 pockets are to be deposited in the structure region.

In order to make the fourth criteria, construction time, independent of the number of pockets, we modify this criteria by dividing the construction time by the number of the total deposited pockets. This value is called average iteration time. Fig. 5.2
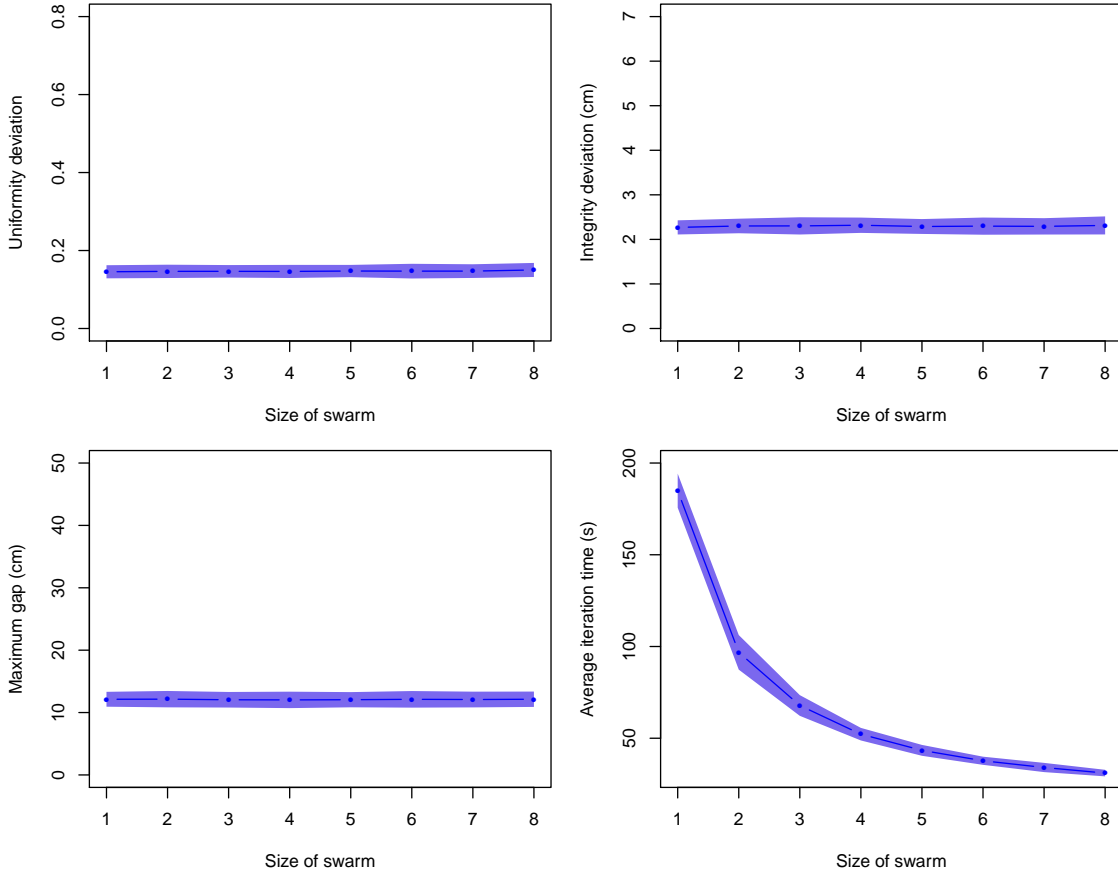
FIGURE 5.3: Scalability analysis: the effect of the size of the swarm on the performance criteria (represented by the mean and standard deviation of experimental data).

shows the results of multi-robot simulation experiments with 5 robots in the new setup with those of single robot simulation experiments in the previous setup with the same occlusion threshold (that is, 75%). The results for the first three criteria show that the quality of the longer structure (350 cm) is roughly similar to that of the shorter structure (100 cm). The results for the fourth criterion, that is, average iteration time, for these experiments is also shown. Note that the results for average iteration time are different due to the fact that the number of robots and the size of the arena have changed.

For scalability analysis, we ran simulation experiments in the new setup for group
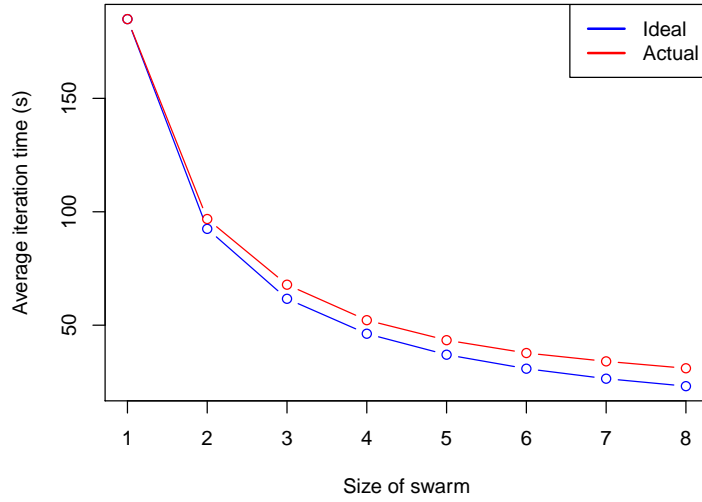
FIGURE 5.4: Average iteration time as a function of the size of the swarm for ideal swarm construction system and actual swarm construction system.

sizes ranging from 1 to 8 robots. Fig. 5.3 illustrates the mean and standard deviation of the four criteria for different group sizes. As can be seen, the quality of the built structure in terms of uniformity deviation, integrity deviation, and maximum gap almost stays constant by increasing the number of robots. This means that, despite the presence of interference in multi-robot experiments, the final structure is similar to the one built by a single robots. However, the average construction time decreases rapidly. This decrement in the construction time shows the significant advantage of the cooperation between the robots in the accomplishment of the common task.

5.3 Swarm construction system efficiency

In this section, we study the efficiency of our swarm construction system. As said earlier, interference between robots degrades the performance of each robot in the multi-robot system with respect to the single robot system. In order to understand the influence of the interference, we need to measure this degradation.

In the ideal condition, we can imagine that the increment of the size of the
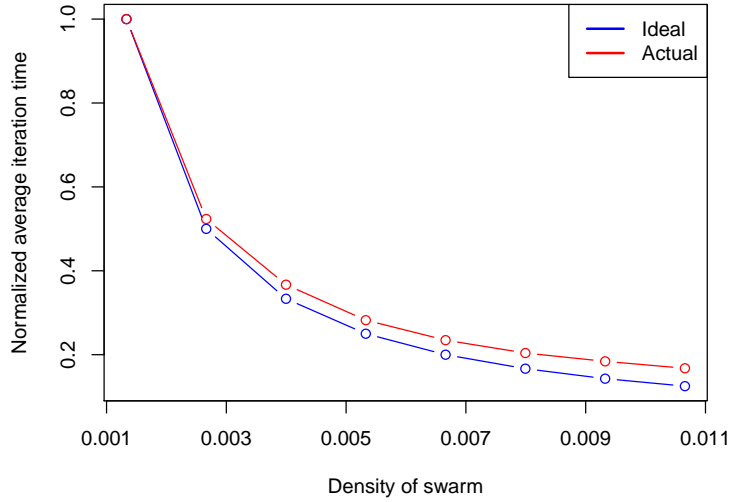
FIGURE 5.5: Normalized average iteration time as a function of the density of the swarm for ideal swarm construction system and actual swarm construction system.

swarm does not affect the performance of each robot. Therefore, the interference does not exist. In this condition, each robot in the multi-robot system has the same performance as that of the robot in the single robot system. Thus, the construction time in the multi-robot system, decreasing due to the increment of the size of the swarm, can be obtained by dividing the construction time in the single robot system by the size of the swarm. Let $\xi_d(m)$ denote the average iteration time in the ideal swarm construction system with m robots, and $\xi_c(m)$ denote the average iteration time in the actual swarm construction system with m robots. The average iteration time for the ideal system is given by

$$\xi_d(m) = \frac{\xi_c(1)}{m} \tag{5.1}$$

where $\xi_c(1)$ is the average iteration time in the actual system with a single robot, that is available, and m is the size of the swarm. Note that $\xi_d(1) = \xi_c(1)$ where $\xi_d(1)$ is the average iteration time in the ideal system with a single robot. Fig. 5.4 illustrates the average iteration time for ideal and actual systems versus the size of

38
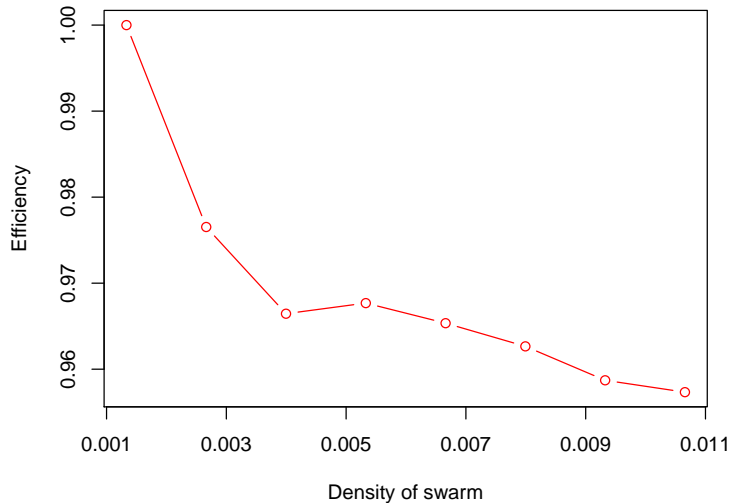
FIGURE 5.6: Efficiency of the proposed swarm construction system as a function of the density of the swarm.

the swarm (based on the mean of the experimental data of Fig. 5.3). It can be seen that, as expected, the actual system has greater average iteration time than the ideal system. This difference shows the performance degradation due to the interference. Before concentrating on this difference, we operate a change in the variables.

In fact, the interference between the robots does not exactly depend on the size of the swarm, but rather on the density of the swarm. The interference increases when the density of the swarm increases. The density of the swarm is a function of the size of the swarm and of the size of the arena, and can be defined as

$$\rho_s = \frac{\pi R^2 m}{A_a} \tag{5.2}$$

where R is the radius of each robot, and A_a is the effective area of the arena.

We normalize the average iteration time by dividing it by the average iteration time of a single robot system

$$\bar{\xi}_d(m) = \frac{\xi_d(m)}{\xi_d(1)}, \quad \bar{\xi}_c(m) = \frac{\xi_c(m)}{\xi_d(1)} \tag{5.3}$$

39

where $\bar{\xi}_d(m)$ and $\bar{\xi}_c(m)$ are the normalized average iteration times for ideal and actual systems, respectively. Fig. 5.5 illustrates the normalized average iteration time for ideal and actual systems versus the density of the swarm.

We define the efficiency of a swarm construction system based on the normalized average iteration time for ideal and actual systems as

$$\eta_s(\rho_s) = 1 - \left(\bar{\xi}_c(\rho_s) - \bar{\xi}_d(\rho_s) \right) \tag{5.4}$$

The efficiency represents the performance degradation caused by the interference. If the interference is zero (the ideal condition), the efficiency is equal to 1, and if the interference grows, the efficiency decreases. Fig. 5.6 shows the efficiency of our swarm construction system for different densities of the swarm. As seen, the diagram has a general decreasing trend with the increase of the density. Although there is an unusual increment in the efficiency around the density 0.005, the change is very small, and we expect that it will vanish if one increases the number of the experiment trials. Note that the efficiency of our swarm construction system for the reported densities is very high, that is, more that 95%. Based on this result, we can confirm that the proposed swarm construction system works very closely to the ideal system.

6

Conclusions

In this work, we developed a bio-inspired autonomous construction system. We employed autonomous ground robots to build a protective barrier using deformable pockets as the building material.

We provided a reactive control algorithm for the autonomous robot that exploits the advantages of deformable pockets. We defined two stochastic mechanisms based on the set of locally visible pockets which determine the probability of choosing the deposition point. One mechanism allows the robot to explore the structure along the length, build it uniformly, and fill voids. The other mechanism permits the robot to maximize the compactness of the structure along the width, and build it coherently. In order to implement the algorithm in a swarm of robots, we modified the algorithm, and resolved the robot interference problem.

We proposed a probabilistic method for representation of the resulting structures and for the investigation of their properties. We defined a set of criteria for assessing the quality of the structures and the proposed construction system.

We defined a scenario to realize the task in our laboratory arena and carried out real-robot experiments. The results of the real-robot experiments demonstrated

the performance of our autonomous construction system in accomplishing the task objective.

We developed a simulation model for the pockets, and validated our simulation. This allowed us to carry out multi-robot simulation experiments. We analyzed the effect of the size of the swarm on the performance criteria. The results showed the significant advantage of the cooperation between robots in the accomplishment of the common task. Then, we compared the performance of our swarm construction system with the ideal swarm construction system. Finally, we measured the efficiency of our swarm construction system. Based on the results, we confirmed that the proposed swarm construction system works closely to an ideal system without inter-robot interference.

From the experiments we performed, we can conclude that deformable pockets are particularly suited for a simple stochastic deployment as it is not necessary to finely control their positioning and alignment. Indeed, by simply implementing local probabilistic rules, we achieved the construction of uniform, packed and coherent structures. This would be very difficult with rigid objects, and it would require for sure more complex hardware and control algorithm. We believe that the use of deformable materials is very appropriate for a group of applications of autonomous construction in unstructured environments.

In the other hand, reactive and stochastic controllers can be easily adopted in swarm robotics systems. Employing swarm robotics systems with their unique features such as scalability, robustness, and adaptivity in autonomous construction will result in highly efficient multi-robot construction.

Bibliography

Abderrahim, M. and Balaguer, C. (2007), *Robotics and Automation Technologies in Construction*, vol. 4, International Journal of Advanced Robotic Systems.

Bell, J., D. Lail, C. M., and Nguyen, P. (2011), "Radiation Shielding for a Lunar Base," National Aeronautics and Space Adiminstration.

Bonani, M., Longchamp, V., Magnenat, S., Retornaz, P., Burnier, D., Roulet, G., Vaussard, F., Bleuler, H., and Mondada, F. (2010), "The marXbot, a miniature mobile robot opening new perspectives for the collective-robotic research," in *Intelligent Robots and Systems (IROS), 2010 IEEE/RSJ International Conference on*, pp. 4187–4193.

Brooks, R., Maes, P., Mataric, M., and More, G. (1990), "Lunar base construction robots," in *Intelligent Robots and Systems '90. 'Towards a New Frontier of Applications', Proceedings. IROS '90. IEEE International Workshop on*, pp. 389–392 vol.1.

Cannon, R., Henninger, S., Levandoski, M., Perkins, J., Pitchon, J., Swats, R., and Wessels, R. (1990), "Lunar Regolith Bagging System," NASA/USRA Advanced Design Program.

Dorigo, M. and Sahin, E. (2004), "Guest Editorial. Special Issue: Swarm Robotics," *Autonomous Robots*, 17, 111–113.

Dorigo, M., Floreano, D., Gambardella, L. M., Mondada, F., Nolfi, S., Baaboura, T., Birattari, M., Bonani, M., Brambilla, M., Brutschy, A., Burnier, D., Campo, A., Christensen, A., Decugnire, A., Di Caro, G., Ducatelle, F., Ferrante, E., Frster, A., Guzzi, J., Longchamp, V., Magnenat, S., Martinez Gonzales, J., Mathews, N., Montes de Oca, M., O'Grady, R., Pinciroli, C., Pini, G., Rtornaz, P., Roberts, J., Sperati, V., Stirling, T., Stranieri, A., Stützle, T., Trianni, V., Tuci, E., Turgut, A. E., and Vaussard, F. (2013), "Swarmanoid: a novel concept for the study of heterogeneous robotic swarms," *IEEE Robotics & Automation Magazine*, p. in press.

Ducatelle, F., Di Caro, G., Pinciroli, C., Mondada, F., and Gambardella, L. (2011), "Communication assisted navigation in robotic swarms: Self-organization and co-

operation," in *Intelligent Robots and Systems (IROS), 2011 IEEE/RSJ International Conference on*, pp. 4981–4988.

Grassé, P.-P. (1959), "La reconstruction du nid et les coordinations interindividuelles chez Bellicositermes natalensis et Cubitermes sp. La theorie de la stigmergie: Essai dinterpretation du comportement des termites constructeurs," *Insectes Sociaux*, 6, 41–81.

Khalili, N. (2011), *Emergency Sandbag Shelter and Eco-Village: Manual-How to Build Your Own with Superadobe/Earthbags*, Cal Earth Press.

Khoshnevis, B., Kim, W., Toutanji, H., and Fiske, M. R. (2010), "Lunar contour craftingA novel technique for ISRU-based habitat development," American Institute of Aeronautics and Astronautics Conference (AIAA).

Lindsey, Q., Mellinger, D., and Kumar, V. (2012), "Construction with quadrotor teams," *Autonomous Robots*, 33, 323–336.

Magnenat, S., Philippsen, R., and Mondada, F. (2012), "Autonomous construction using scarce resources in unknown environments," *Autonomous Robots*, 33, 467–485.

Melhuish, C., Welsby, J., and Edwards, C. (1999), "Using templates for defensive wall building with autonomous mobile ant-like robots," in *towards intelligent autonomous mobile robots*.

Napp, N. and Nagpal, R. (2012), "Distributed Amorphous Ramp Construction in Unstructured Environments," Symposium on Distributed Autonomous Robotic Systems (DARS).

Napp, N., Rappoli, O., Wu, J., and Nagpal, R. (2012), "Materials and mechanisms for amorphous robotic construction," in *Intelligent Robots and Systems (IROS), 2012 IEEE/RSJ International Conference on*, pp. 4879–4885.

Petersen, K., Nagpal, R., and Werfel, J. (2011), "TERMES: An Autonomous Robotic System for Three-Dimensional Collective Construction," in *Proceedings of Robotics: Science and Systems*, Los Angeles, CA, USA.

Pinciroli, C., Trianni, V., O'Grady, R., Pini, G., Brutschy, A., Brambilla, M., Mathews, N., Ferrante, E., Di Caro, G., Ducatelle, F., Birattari, M., Gambardella, L. M., and Dorigo, M. (2012), "ARGoS: a Modular, Parallel, Multi-Engine Simulator for Multi-Robot Systems," *Swarm Intelligence*, 6, 271–295.

Pini, G., Brutschy, A., Pinciroli, C., Dorigo, M., and Birattari, M. (2013), "Autonomous task partitioning in robot foraging: an approach based on cost estimation," *Adaptive Behavior*, 21, 118–136.

Revzen, S., Bhoite, M., Macasieb, A., and Yim, M. (2011), "Structure synthesis on-the-fly in a modular robot," in *Intelligent Robots and Systems (IROS), 2011 IEEE/RSJ International Conference on*, pp. 4797–4802.

Smithers, G. A., Nehls, M. K., Hovater, M. A., Evans, S. W., Miller, J. S., Jr, R. M. B., Beale, D., and Kilinc-Balci, F. (2007), "A One-Piece Lunar Regolith Bag Garage Prototype," In Space Resources Roundtable VIII: Program and Abstracts (LPI Contribution No. 1332), NASA.

Theraulaz, G., Gautrais, J., Camazine, S., and Deneubourg, J. L. (2003), "The formation of spatial patterns in social insects: from simple behaviours to complex structures," *Philosophical Transactions of the Royal Society of London. Series A: Mathematical, Physical and Engineering Sciences 361*.

Wand, M. P. and Jones, M. C. (1995), *Kernel Smoothing*, vol. 4, Chapman and Hall.

Wawerla, J., Sukhatme, G., and Mataric, M. (2002), "Collective construction with multiple robots," in *Intelligent Robots and Systems, 2002. IEEE/RSJ International Conference on*, vol. 3, pp. 2696–2701.

Willmann, J., Augugliaro, F., Cadalbert, T., D'Andrea, R., Gramazio, F., and Kohler, M. (2012), "Aerial Robotic Construction: Towards a New Field of Architectural Research," *International journal of architectural computing*, 10-3, 439.

Wismer, S., Hitz, G., Bonani, M., Gribovskiy, A., and Magnenat, S. (2012), "Autonomous construction of a roofed structure: Synthesizing planning and stigmergy on a mobile robot," in *Intelligent Robots and Systems (IROS), 2012 IEEE/RSJ International Conference on*, pp. 5436–5437.